

# Inverse Faraday Effect in Rashba two-dimensional electron systems: interplay of spin and orbital effects

Jaglul Hasan<sup>1,2</sup> and Chandan Setty<sup>1,2</sup>

<sup>1</sup>*Department of Physics and Astronomy, Iowa State University, Ames, Iowa 50011, USA*

<sup>2</sup>*Ames National Laboratory, U.S. Department of Energy, Ames, Iowa 50011, USA*

(Dated: March 16, 2026)

The inverse Faraday effect (IFE) refers to the generation of a dc magnetization by circularly polarized light through the transfer of optical angular momentum to electronic degrees of freedom. In conducting systems this response can arise from two microscopic channels: spin polarization of itinerant electrons and orbital magnetization generated by circulating charge currents. However, the orbital contribution to the inverse Faraday effect in spin-orbit-coupled conducting systems remains largely unexplored. We present a theoretical analysis of the IFE in disordered two-dimensional electron systems with Rashba spin-orbit coupling using both the quantum kinetic equation and Green's-function diagrammatics. We find that in a noninteracting Rashba metal the orbital magnetization is strongly modified by spin-orbit coupling and can become comparable to, or exceed the spin magnetization for realistic parameter regimes. When the radiation frequency approaches the Rashba spin splitting, both spin and orbital magnetizations exhibit resonant enhancement. These results clarify the microscopic origin of light-induced magnetization and highlight the interplay of spin and orbital mechanisms in optically driven magnetization dynamics in low-dimensional electronic systems.

## I. INTRODUCTION

Circularly polarized light carries angular momentum, and its transfer to matter can generate a dc axial response proportional to the optical helicity, represented by the axial vector  $i[\mathbf{E}(\omega) \times \mathbf{E}^*(\omega)]$ , where  $\mathbf{E}(\omega)$  is the complex electric-field amplitude at frequency  $\omega$ . Using thermodynamic arguments, Pitaevskii [1] showed that rotating electric fields, such as those associated with circular or elliptical polarization, induce off-diagonal components of the dielectric tensor in dispersive media that are linear in the magnetic field, giving rise to a light-induced magnetization proportional to this axial vector. This phenomenon was subsequently observed experimentally in liquids and solids [2–4] and became known as the inverse Faraday effect (IFE).

Microscopic interpretations soon followed, relating the effect to nonlinear optical processes or Raman-type light-matter interactions that generate magnetization [5–11]. From a microscopic viewpoint, the induced response can arise from two mechanisms: orbital magnetization associated with helicity-driven circulating charge currents and spin polarization of electronic states. Understanding the relative importance of these two channels has therefore become central to interpreting inverse Faraday experiments. These ideas underpin a variety of ultrafast magneto-optical phenomena, including coherent spin manipulation and nonthermal magnetization control by femtosecond laser pulses [12–18]. In modern ultrafast experiments the IFE often appears as a transient effective magnetic field capable of driving magnetization dynamics in gaseous He atoms [19], ionic liquids [20], insulators, semiconductors, and metals [21–23], enabling helicity-dependent all-optical switching in ferro- and antiferromagnets [24–26], and even controlling the topological Chern number in moiré quantum materials

[27].

In conducting systems the orbital contribution to the IFE arises from intrinsically nonequilibrium electronic dynamics governed by absorption, dissipation, and light-driven charge motion. A semiclassical description for metals was proposed by Hertel [28], who showed that circularly polarized light drives electrons along solenoidal trajectories that produce circulating charge currents and an associated orbital IFE. Related microscopic pictures based on electron drift motion and plasma dynamics have also been developed [29–31]. Related orbital mechanisms have since been discussed in a broad range of systems, including magnetic materials [32, 33], superconductors [34–38], Dirac and Weyl materials [39], correlated systems [40], and plasmonic nanostructures where local field enhancement can dramatically amplify the effect [41–46]. In such nanostructured environments, circulating surface currents and plasmonic resonances can generate strong effective magnetic fields and enable nanoscale control of magnetization [47–54].

A second microscopic route to the IFE is the spin channel: Edelstein predicted that in noncentrosymmetric conductors with strong spin-orbit coupling (SOC), circularly polarized light can generate a nonequilibrium spin polarization of conduction electrons [55]. This mechanism is closely related to the dc Edelstein magnetoelectric effect, in which an electric current produces spin polarization in inversion-asymmetric conductors [56–58]. In Rashba and other spin-orbit-coupled conductors—including systems with and without inversion symmetry—the optical analogue of this effect produces a helicity-dependent spin magnetization proportional to the optical helicity and controlled by scattering and relaxation processes [59–65]. However, finite dissipation due to disorder or external magnetic fields has often been invoked as a mechanism enabling a dc response in

time-reversal-symmetric systems. Because the induced magnetization in these treatments arises from spin polarization generated through SOC, the IFE in Rashba metals has generally been interpreted primarily in terms of a spin response, with orbital charge dynamics not treated as an independent contribution to the magnetization [59, 60].

Nevertheless, ultrafast pump-probe measurements indicate that the induced magnetization can arise from light-driven orbital currents on femtosecond time scales rather than spin polarization of the charge carriers [18], while recent microscopic theories of metals and superconductors emphasize the role of circulating charge currents and orbital magnetic moments in generating the inverse Faraday response [66–69]. These results suggest that orbital dynamics may contribute to the inverse Faraday response on the same footing as spin polarization, raising the question of how spin and orbital channels compete in spin-orbit-coupled conductors. However, despite these developments, the orbital inverse Faraday response in spin-orbit-coupled conductors has not been systematically analyzed, particularly in systems where SOC itself strongly modifies the charge dynamics. In particular, although circulating currents provide the natural microscopic origin of orbital magnetization, existing treatments of IFE in Rashba systems typically yield responses that scale with SOC strength and therefore do not reproduce the established orbital IFE of normal metals in the limit of vanishing SOC.

In this work we show that the inverse Faraday effect in a Rashba two-dimensional electron gas contains two distinct contributions: (i) a spin magnetization arising from nonequilibrium spin polarization of itinerant electrons, and (ii) an orbital magnetization originating from light-induced circulating motion of charge carriers. While both are proportional to the optical helicity, they originate from different microscopic mechanisms. These distinctions are particularly relevant in the ultrafast optical regime, where intense THz and femtosecond radiation drive electronic dynamics far from equilibrium [70, 71].

Our central results are obtained by combining a quantum kinetic description of light-driven charge currents with an explicit evaluation of spin polarization using both the Wigner distribution formalism [68, 72–74] and Edelman’s diagrammatic approach [55]. Within this framework we identify the spin and orbital contributions to the inverse Faraday response separately. We demonstrate that in a noninteracting Rashba metal the orbital inverse Faraday effect is substantially reshaped by SOC and can become comparable to, or exceed, the spin contribution for realistic values of disorder and radiation frequency. These results clarify the microscopic origin of light-induced magnetization in spin-orbit-coupled metals and provide a useful reference point for nonlinear optical responses in low-dimensional electronic systems [75–80].

## II. MODEL AND TECHNICAL APPROACH

We consider noninteracting electrons confined to a plane and subject to Rashba SOC, a time-dependent vector potential  $\mathbf{A}$ , and a disorder potential. The Hamiltonian is

$$\hat{H}(\mathbf{r}, t) = \frac{1}{2m} \left[ \hat{\mathbf{p}} - \frac{e}{c} \mathbf{A}(\mathbf{r}, t) \right]^2 + \alpha_{\text{so}} (\mathbf{c} \times \hat{\boldsymbol{\sigma}}) \cdot \left( \hat{\mathbf{p}} - \frac{e}{c} \mathbf{A}(\mathbf{r}, t) \right) + U(\mathbf{r}). \quad (1)$$

Here,  $\hat{\mathbf{p}} = -i\nabla$  is the electron momentum,  $\mathbf{c}$  is the unit vector along the direction of the asymmetric potential gradient perpendicular to the 2D metal,  $\hat{\boldsymbol{\sigma}}$  is Pauli spin matrix-vector,  $U(\mathbf{r})$  is the disorder potential, and  $\mathbf{A}(\mathbf{r}, t)$  is the vector potential corresponding to the periodically modulated electric field,  $\mathbf{E} = -(1/c)\partial_t \mathbf{A} = \mathbf{E}_0 e^{i(\mathbf{q}\mathbf{r} - \omega t)} + \text{c.c.}$  Throughout this work we use units with  $\hbar = k_B = 1$ . For simplicity, we assume a short-range disorder potential generated by pointlike impurities with Gaussian white-noise correlations,

$$\langle U(\mathbf{r})U(\mathbf{r}') \rangle = \frac{\delta(\mathbf{r} - \mathbf{r}')}{2\pi\nu_F\tau}, \quad (2)$$

where angular brackets denote averaging over disorder. The disorder scattering rate is  $\tau^{-1}$  and  $\nu_F = m/2\pi$  is the single-particle density of states (per spin). We consider a circularly polarized electromagnetic wave,  $\mathbf{E}_0 = E_0(\mathbf{e}_x + i\mathbf{e}_y)$  where  $\mathbf{e}_{x,y}$  are the unit vectors along the  $x$  and  $y$  axes respectively. As shown below, a static magnetization proportional to  $|\mathbf{E}_0|^2$  arises only for circular polarization within the present model. To determine physical observables such as the electric current density and the orbital and spin magnetizations, we calculate the electronic distribution function. Here, following Refs. [68, 72, 73, 81], we use the Wigner distribution function (WDF), which is a  $2 \times 2$  matrix in spin space defined by

$$\hat{w}_{\mathbf{k}\varepsilon}(\mathbf{r}, t) = \frac{1}{2\pi} \int d^2\mathbf{s} \int d\tau e^{i\mathbf{k}\mathbf{s} - i\varepsilon\tau} \times \left\langle \psi_{\beta}^{\dagger} \left( \mathbf{r} + \frac{\mathbf{s}}{2}, t + \frac{\tau}{2} \right) \psi_{\alpha} \left( \mathbf{r} - \frac{\mathbf{s}}{2}, t - \frac{\tau}{2} \right) \right\rangle. \quad (3)$$

The kinetic equation for this distribution function is obtained from the Dyson equations for the Keldysh Green’s functions using a Wigner transformation and retaining leading gradients in space and time [68]. The derivation assumes (i) the quasiclassical approximation near the Fermi surface,  $|\mathbf{k}| \approx k_F$ , (ii) slowly varying electromagnetic fields in space and time, allowing truncation of the gradient expansion at first order, (iii) weak spin-orbit coupling  $\alpha_{\text{so}} \ll v_F$ , and (iv) elastic impurity scattering treated in the Born approximation with a relaxation time  $\tau$ . Within these approximations, the Wigner distribution function obeys the kinetic equation

$$\begin{aligned} & \left( \partial_t + \frac{\mathbf{k} \cdot \nabla}{m} + \frac{1}{\tau} \right) \hat{w}_{\mathbf{k}\varepsilon} + i\alpha_{\text{so}} [(\mathbf{k} \times \mathbf{c}) \cdot \hat{\boldsymbol{\sigma}}, \hat{w}_{\mathbf{k}\varepsilon}] = -\frac{1}{2} \left\{ \frac{\mathbf{k}}{m} + \alpha_{\text{so}} (\mathbf{c} \times \hat{\boldsymbol{\sigma}}), \bar{\nabla} \hat{w}_{\mathbf{k}\varepsilon} \right\} - \frac{e\alpha_{\text{so}}}{2\omega} [(\mathbf{c} \times \hat{\boldsymbol{\sigma}}), \hat{\gamma}_{\omega}(\mathbf{k}\varepsilon; \mathbf{r}t)] \delta \mathbf{E}(\mathbf{r}, t) \\ & - \frac{\alpha_{\text{so}}}{2} \{(\mathbf{c} \times \hat{\boldsymbol{\sigma}}), \nabla \hat{w}_{\mathbf{k}\varepsilon}\} + \frac{i}{2\pi v_F \tau} \int \frac{d^2 \mathbf{k}}{(2\pi)^2} \left[ \hat{G}_{\mathbf{k}\varepsilon}^R(\mathbf{r}, t) \circ \hat{w}_{\mathbf{k}\varepsilon}(\mathbf{r}, t) - \hat{w}_{\mathbf{k}\varepsilon}(\mathbf{r}, t) \circ \hat{G}_{\mathbf{k}\varepsilon}^A(\mathbf{r}, t) \right], \end{aligned} \quad (4)$$

where  $\delta \mathbf{E}(\mathbf{r}, t) = \mathbf{E}_0 e^{i(\mathbf{q}\mathbf{r} - \omega t)} - \mathbf{E}_0^* e^{-i(\mathbf{q}\mathbf{r} - \omega t)}$ ,  $\hat{G}_{\mathbf{k}\varepsilon}^{R(A)}$  are retarded (advanced) Green's functions and

$$\bar{\nabla} \hat{w}_{\mathbf{k}\varepsilon} = \frac{e}{\omega} (\hat{w}_{\mathbf{k}\varepsilon + \frac{\omega}{2}} - \hat{w}_{\mathbf{k}\varepsilon - \frac{\omega}{2}}) \mathbf{E}(\mathbf{r}, t). \quad (5)$$

In such systems with SOC, circularly polarized light can generate a dc magnetization carried either by the *spin* degree of freedom or by *circulating charge motion*. The spin contribution is obtained directly from the spin-dependent Wigner distribution function,

$$\mathbf{M}_{\text{spin}}(\mathbf{r}, t) = \frac{g\mu_B}{2} \int_{\mathbf{k}, \varepsilon} \text{Tr}[\boldsymbol{\sigma} \hat{w}_{\mathbf{k}\varepsilon}(\mathbf{r}, t)] \equiv g\mu_B \mathbf{S}(\mathbf{r}, t), \quad (6)$$

where  $\int_{\mathbf{k}, \varepsilon} = \int_0^\infty \frac{k dk}{2\pi} \int_0^{2\pi} \frac{d\theta}{2\pi} \int_{-\infty}^\infty d\varepsilon$ . The spin magnetization  $\mathbf{M}_{\text{spin}}$  can equivalently be obtained from Edelman's diagrammatic approach shown in Fig. 1. By con-

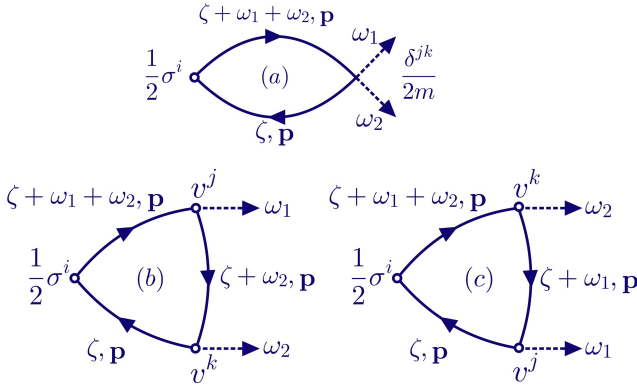


FIG. 1. The diagrams responsible for spin IFE.

trast, orbital magnetization is associated with circulating charge motion and must therefore be obtained from the curl component of the induced current density rather than from a local trace of the Wigner distribution function or the diagrammatic expansion of a local observable. The electric current density is given by

$$\mathbf{j}(\mathbf{r}, t) = e \int_{\mathbf{k}, \varepsilon} \text{Tr}[\mathbf{v}(\mathbf{k}) \hat{w}_{\mathbf{k}\varepsilon}(\mathbf{r}, t)], \quad (7)$$

where  $\mathbf{v}$  is the velocity operator, which, along with the usual scalar part, also has a spin component:

$$\mathbf{v}_{ab}(\mathbf{k}) = i [\mathcal{H}_{ab}(\mathbf{k}), \mathbf{r}] = \frac{\mathbf{k}}{m} \delta_{ab} + \alpha_{\text{so}} (\mathbf{c} \times \boldsymbol{\sigma})_{ab}, \quad (8)$$

with  $a, b$  being spin indices. This definition differs from that used in Refs. [68, 73], where the SOC term

in the velocity operator is neglected under the assumption  $\alpha/v_F \ll 1$ . Accordingly, the orbital magnetization is extracted operationally from the *magnetization (curl) current* at second order in the optical field,

$$\mathbf{j}_{\text{IFE}}^{(2)}(\mathbf{r}) = \nabla \times \mathbf{M}_{\text{orb}}(\mathbf{r}), \quad (9)$$

where only the transverse (circulating) part of the second-order current is retained. For the two-dimensional geometry considered here, the corresponding orbital magnetization is directed along  $\mathbf{c}$ . Equation (8) naturally decomposes the current  $\mathbf{j} = \mathbf{j}_0 + \mathbf{j}_{\text{soc}}$  into a canonical contribution  $\mathbf{j}_0 = e \int_{\mathbf{k}, \varepsilon} (\mathbf{k}/m) \text{Tr}[\hat{w}_{\mathbf{k}\varepsilon}]$  and an SOC-velocity contribution  $\mathbf{j}_{\text{soc}} = e \int_{\mathbf{k}, \varepsilon} \text{Tr}[\alpha_{\text{so}} (\mathbf{c} \times \boldsymbol{\sigma}) \hat{w}_{\mathbf{k}\varepsilon}]$ . This decomposition is useful for organizing the orbital response: it separates the normal-metal baseline associated with the canonical current from SOC-enabled corrections arising from the spin-dependent velocity, while the SOC-gradient (convective) term in the kinetic equation modifies the nonequilibrium distribution entering these currents. In what follows, orbital contributions are extracted from the curl component of  $\mathbf{j}^{(2)}$  via Eq. (9).

In thermal equilibrium, in the absence of spin-orbit coupling ( $\alpha_{\text{so}} = 0$ ) and disorder, the Wigner distribution function reduces to

$$w_{\mathbf{k}\varepsilon, ab} = f_0(\varepsilon) \delta(\varepsilon - \varepsilon_{\mathbf{k}}) \delta_{ab}, \quad (10)$$

where  $f_0$  is the Fermi function. For finite spin-orbit coupling ( $\alpha_{\text{so}} \neq 0$ ) the Rashba interaction lifts the spin degeneracy and splits the spectrum into two helical branches with energies which, on the assumption of the isotropic electron mass, are  $\varepsilon_{\mathbf{k}\lambda} = \frac{k^2}{2m} + \lambda \alpha_{\text{so}} k$  with  $\lambda = \pm 1$ . Thus one finds in equilibrium,  $w_{\mathbf{k}\varepsilon, ab} = w_{\mathbf{k}\varepsilon, ab}^{(0)}$  with

$$w_{\mathbf{k}\varepsilon, ab}^{(0)} = \frac{1}{2} \sum_{\lambda=\pm 1} \left[ \delta_{ab} + \lambda (\hat{\mathbf{k}} \times \mathbf{c}) \cdot \boldsymbol{\sigma}_{ab} \right] f_0(\varepsilon) \delta(\varepsilon - \varepsilon_{\mathbf{k}\lambda}). \quad (11)$$

We solve the kinetic equation perturbatively in the electric field and spatial gradients. Small gradient terms are moved to the right-hand side of the kinetic equation (4), so that the left-hand side describes rapid relaxation toward the local equilibrium distribution:

$$\left( \partial_t + \frac{\mathbf{k} \cdot \nabla}{m} + \frac{1}{\tau} \right) \hat{w}_{\mathbf{k}\varepsilon} + i\Delta_k [\hat{\eta}_{\mathbf{k}}, \hat{w}_{\mathbf{k}\varepsilon}] = \hat{\mathcal{K}}_{\mathbf{k}\varepsilon} \hat{w}_{\mathbf{k}\varepsilon} \equiv \hat{\mathcal{K}}_{\mathbf{k}\varepsilon}^{(1)} \hat{w}_{\mathbf{k}\varepsilon} + \hat{\mathcal{K}}_{\mathbf{k}\varepsilon}^{(2)} \hat{w}_{\mathbf{k}\varepsilon}, \quad (12)$$

where

$$\hat{\mathcal{K}}_{\mathbf{k}\varepsilon}^{(1)} [\hat{w}_{\mathbf{k}\varepsilon}] = -\frac{1}{2} \left\{ \frac{\mathbf{k}}{m} + \alpha \hat{\eta}, \bar{\nabla} \hat{w}_{\mathbf{k}\varepsilon} \right\},$$

$$\hat{\mathcal{K}}_{\mathbf{k}\varepsilon}^{(2)}[\hat{w}_{\mathbf{k}\varepsilon}] = -\frac{\alpha_{so}}{2} \{(\mathbf{c} \times \hat{\boldsymbol{\sigma}}), \nabla \hat{w}_{\mathbf{k}\varepsilon}\}, \quad (13)$$

with  $\Delta_k = \alpha_{so}k$  and  $\hat{\eta}_{\mathbf{k}} = (\hat{\mathbf{k}} \times \mathbf{c}) \cdot \hat{\boldsymbol{\sigma}}$  and  $\bar{\nabla} \hat{w}_{\mathbf{k}\varepsilon}$  defined in Eq. (5). Both the radiation-induced source term  $\hat{\mathcal{K}}_{\mathbf{k}\varepsilon}^{(1)}$  and the gradient contribution  $\hat{\mathcal{K}}_{\mathbf{k}\varepsilon}^{(2)}$  represent small deviations from local equilibrium and can therefore be treated perturbatively. In the Fourier representation with respect to time, the formal solution of Eq. (12) can be written as,

$$\begin{aligned} \hat{w}_{\mathbf{k}\varepsilon} &= i \frac{(2\Delta_k^2 - \Omega^2)\hat{\mathcal{K}}_{\mathbf{k}\varepsilon} + 2\Delta_k^2 \hat{\eta}_{\mathbf{k}} \hat{\mathcal{K}}_{\mathbf{k}\varepsilon} \hat{\eta}_{\mathbf{k}} - \Omega \Delta_k [\hat{\eta}_{\mathbf{k}}, \hat{\mathcal{K}}_{\mathbf{k}\varepsilon}]}{\Omega(4\Delta_k^2 - \Omega^2)} \\ &\equiv \mathcal{L}[\hat{\mathcal{K}}_{\mathbf{k}\varepsilon}], \end{aligned} \quad (14)$$

where  $\Omega = \omega + i/\tau$ . To first order, the equilibrium distribution  $\hat{w}_{\mathbf{k}\varepsilon}^{(0)}$  from Eq. (11) is substituted into the source term  $\hat{\mathcal{K}}_{\mathbf{k}\varepsilon}^{(1)}$ , yielding the first correction  $\hat{w}_{\mathbf{k}\varepsilon}^{(1)}$ . This procedure is then to be repeated to the necessary order,

$$\begin{aligned} \hat{w}_{\mathbf{k}\varepsilon}^{(1)} &= \mathcal{L} \left[ \hat{\mathcal{K}}_{\mathbf{k}\varepsilon}^{(1)}[\hat{w}_{\mathbf{k}\varepsilon}^{(0)}] \right], \\ \hat{w}_{\mathbf{k}\varepsilon}^{(i)} &= \hat{w}_{\mathbf{k}\varepsilon}^{(i-1)} + \mathcal{L} \left[ \hat{\mathcal{K}}_{\mathbf{k}\varepsilon}^{(1)}[\hat{w}_{\mathbf{k}\varepsilon}^{(i-1)}] \right], \quad i \geq 1. \end{aligned} \quad (15)$$

The contribution from the gradient term  $\hat{\mathcal{K}}_{\mathbf{k}\varepsilon}^{(2)}$  can be obtained in a similar way.

### III. RESULTS

We organize the results in three steps. We first establish the orbital inverse Faraday effect in the normal-metal limit without spin-orbit coupling, which provides the reference contribution that must be recovered as  $\alpha_{so} \rightarrow 0$ . We then analyze the spin response in the Rashba system and finally decompose the orbital response in the presence of spin-orbit coupling into three contributions: canonical, convective, and SOC-velocity.

#### A. Orbital IFE in a normal metal

We begin by establishing the orbital IFE in a two-dimensional electron gas (2DEG) without spin-orbit coupling, where spin polarization plays no role. In this limit, circularly polarized light induces a dc magnetization entirely through circulating charge currents, consistent with the semiclassical mechanism originally identified by Hertel [28] and recently reformulated microscopically in Ref. [66]. Within the quantum kinetic description, the orbital magnetization is obtained from the magnetization (curl) component of the nonlinear charge current using Eq. (9) and takes the form

$$\mathbf{M}_{\text{orb}}^{\text{normal}} = \mathcal{M}_{\text{orb}}^{\text{normal}} i (\hat{\mathbf{E}}_0 \times \hat{\mathbf{E}}_0^*), \quad (16)$$

with

$$\mathcal{M}_{\text{orb}}^{\text{normal}} = n_{2D} \mu_B \left( \frac{eE_0}{k_F \varepsilon_F} \right)^2 \mathcal{F} \left( \frac{\omega}{\varepsilon_F}, \varepsilon_F \tau \right), \quad (17)$$

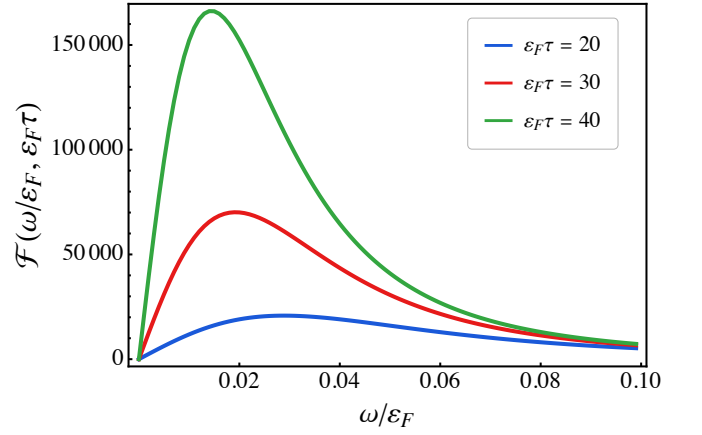


FIG. 2. Plot of orbital IFE magnetization in terms of dimensionless  $\mathcal{F} \left( \frac{\omega}{\varepsilon_F}, \varepsilon_F \tau \right)$  vs light frequency normalized by the Fermi energy,  $\omega/\varepsilon_F$  for different values of  $\varepsilon_F \tau$  in the normal 2DEG without SOC.

where  $n_{2D} = \frac{k_F^2}{2\pi}$ ,  $\mathcal{F}(x, y)$  is a dimensionless function which depends on radiation frequency, Fermi energy and disorder:

$$\mathcal{F}(x, y) = \frac{xy^4}{(1 + (xy)^2)^2}. \quad (18)$$

This resulting orbital magnetization exhibits a characteristic dependence on frequency and disorder: it vanishes in the quasistatic limit ( $\omega \rightarrow 0$ ) as

$$\mathbf{M}_{\text{orb}}^{\text{normal}} \approx \frac{2e^3 \tau^4 \varepsilon_F \omega}{\pi} i (\mathbf{E}_0 \times \mathbf{E}_0^*), \quad (19)$$

and is suppressed at high frequencies as

$$\mathbf{M}_{\text{orb}}^{\text{normal}} \approx \frac{2e^3 \varepsilon_F}{\pi \omega^3} i (\mathbf{E}_0 \times \mathbf{E}_0^*), \quad (20)$$

leading to a pronounced maximum when the driving frequency is comparable to the inverse momentum relaxation time, see Fig. 2. The peak arises from the competition between finite-frequency charge acceleration and impurity-induced momentum relaxation, which together control the build-up of circulating charge currents at  $\omega \sim \tau^{-1}$  (more precisely  $\omega = \frac{1}{\sqrt{3}} \tau^{-1} \approx 0.6 \tau^{-1}$ ). The magnitude of the response depends strongly on the momentum relaxation time  $\tau$ : increasing disorder suppresses the orbital magnetization, while cleaner systems enhance it. This behavior reflects the kinetic origin of the effect, governed by the interplay of finite-frequency driving and momentum relaxation rather than equilibrium band-structure properties. The mechanism itself does not rely on spin-orbit coupling, broken inversion symmetry, or interband transitions, and therefore provides a natural reference point for the analysis of more complex systems with spin-orbit coupling.

This normal metal result serves as a benchmark: any consistent theory of the IFE in systems with SOC

must recover this orbital contribution in the limit where spin-orbit interactions are switched off.

## B. Spin and orbital IFE in Rashba 2DEG

We now turn our attention to a Rashba 2DEG, where spin-orbit coupling introduces additional channels for light-induced magnetization. In this case the inverse Faraday effect contains two contributions: a spin magnetization arising from nonequilibrium spin polarization and an orbital magnetization associated with circulating charge currents.

### 1. Spin IFE in Rashba 2DEG

The Rashba SOC can be interpreted as a Zeeman coupling to a momentum-dependent effective magnetic field

$$\mathbf{B}_f(\mathbf{p}) = \frac{2\alpha_{so}}{\mu_B g_s} (\mathbf{p} \times \mathbf{c}), \quad (21)$$

where  $\mathbf{c}$  denotes the structural inversion-breaking axis. This fictitious field affects electron dynamics in two ways. First, because  $\mathbf{B}_f$  depends on momentum, impurity scattering randomizes its direction and therefore provides an additional channel for spin relaxation. Second, when an electric field drives a charge current  $\mathbf{J} \propto \mathbf{E}$ , the electron ensemble acquires a finite average momentum  $\langle \mathbf{p} \rangle \propto \mathbf{J}$ . The ensemble-averaged effective field  $\langle \mathbf{B}_f \rangle$  then becomes nonzero and induces a uniform spin polarization proportional to  $\mathbf{c} \times \mathbf{E}$  [56]. This magnetoelectric (Edelstein) effect manifests as a first-order field-induced correction to the electronic distribution function ( $\hat{w}_{\mathbf{k}\varepsilon}^{(1)}(\mathbf{r}, t)$  integrated over energy and momentum) proportional to  $\boldsymbol{\sigma} \cdot (\mathbf{c} \times \mathbf{E})$ .

In the present problem the driving field is the radiation field. To second order in the electric-field amplitude, the nonequilibrium correction to the distribution function therefore contains terms bilinear in the optical field. Successive Edelstein-type responses generate a spin-dependent contribution of the form

$$[\boldsymbol{\sigma} \cdot (\mathbf{c} \times \mathbf{E})][\boldsymbol{\sigma} \cdot (\mathbf{c} \times \mathbf{E}^*)]. \quad (22)$$

Using Pauli matrix identities this expression reduces to

$$i(\boldsymbol{\sigma} \cdot \mathbf{c})(\mathbf{c} \cdot \mathbf{E} \times \mathbf{E}^*), \quad (23)$$

which is proportional to the optical helicity  $i(\mathbf{E} \times \mathbf{E}^*)$ . Circularly polarized light therefore generates a time-independent spin polarization along the  $\mathbf{c}$  axis. This mechanism constitutes the spin contribution to the inverse Faraday effect in a Rashba 2DEG. The resulting spin magnetization  $\mathbf{M}_{\text{spin}}$  is obtained from the nonequilibrium spin density, calculated either from the spin-dependent Wigner distribution function (Eq. 6). The full analytic expression (see Appendix A) is plotted in Fig. 3. A resonance peak appears when the radiation

frequency matches the spin splitting at the Fermi surface,  $\omega = 2\alpha_{so}k_F$ . We emphasize that disorder does not generate the spin magnetization; rather it suppresses the response through momentum relaxation. This conclusion is also consistent with the diagrammatic evaluation of the diagrams shown in Fig. 1 in the clean limit.

In the experimentally relevant limit  $\alpha_{so}k_F/\varepsilon_F \ll 1$ , the spin magnetization simplifies to

$$\mathbf{M}_{\text{spin}} = \frac{4e^3\tau^4\alpha_{so}^2\omega}{\pi(1+\omega^2\tau^2)^2} i(\mathbf{E}_0 \times \mathbf{E}_0^*). \quad (24)$$

It vanishes in the quasistatic limit ( $\omega \rightarrow 0$ ) as

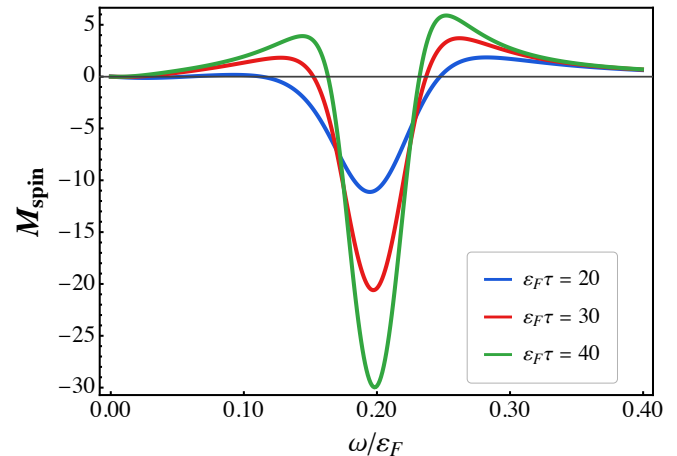


FIG. 3. Plot of dimensionless spin IFE magnetization  $\mathbf{M}_{\text{spin}}$  vs light frequency normalized by the Fermi energy,  $\omega/\varepsilon_F$  for different values of  $\varepsilon_F\tau$  in 2DEG with Rashba SOC for  $\alpha_{so}k_F/\varepsilon_F = 0.1$ .

$$\mathbf{M}_{\text{spin}} \approx \frac{4e^3\tau^4\alpha_{so}^2\omega}{\pi} i(\mathbf{E}_0 \times \mathbf{E}_0^*), \quad (25)$$

and is suppressed at high frequencies as

$$\mathbf{M}_{\text{spin}} \approx \frac{4e^3\alpha_{so}^2}{\pi\omega^3} i(\mathbf{E}_0 \times \mathbf{E}_0^*). \quad (26)$$

### 2. Orbital IFE in Rashba 2DEG

The orbital contribution is obtained from the magnetization (curl) component of the nonlinear charge current, following the same procedure as in the normal-metal case. The full analytic expression is cumbersome (see Appendix A) and is plotted in Fig. 4 after subtracting the normal metal background contribution. Similar to the spin IFE, a resonance peak appears when the radiation frequency matches the spin splitting at the Fermi surface,  $\omega = 2\alpha_{so}k_F$ . In the experimentally relevant limit  $\alpha_{so}k_F/\varepsilon_F \ll 1$ ,

$$\mathbf{M}_{\text{orb}}^{\text{total}} = \frac{2e^3\omega\tau^4}{\pi(1+\omega^2\tau^2)^2} (\varepsilon_F + m\alpha_{so}^2) i(\mathbf{E}_0 \times \mathbf{E}_0^*) \quad (27)$$

Importantly, the orbital inverse Faraday response does not rely on spin polarization and reduces smoothly to the normal-metal result as  $\alpha_{so} \rightarrow 0$ . This continuity demonstrates that the orbital channel is an intrinsic part of the Rashba inverse Faraday response rather than a secondary effect generated by spin dynamics.

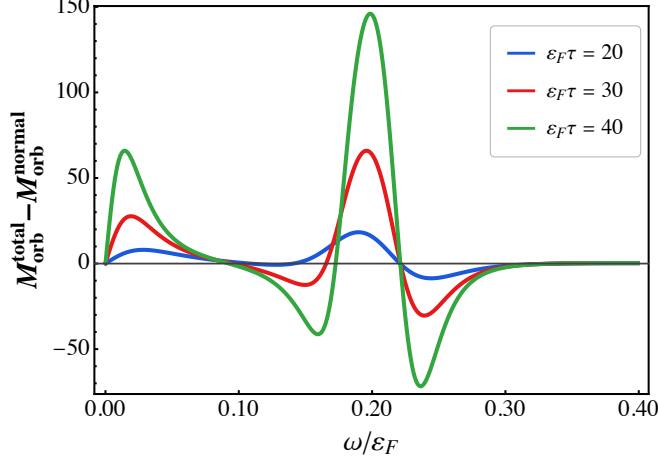


FIG. 4. Plot of dimensionless total orbital IFE magnetization  $M_{\text{orb}}^{\text{total}} - M_{\text{orb}}^{\text{normal}}$  vs light frequency normalized by the Fermi energy,  $\omega/\varepsilon_F$  for different values of  $\varepsilon_F\tau$  in 2DEG with Rashba SOC for  $\alpha_{so}k_F/\varepsilon_F = 0.1$ .

To clarify the origin of the orbital response in the presence of Rashba SOC, it is useful to separate the contributions associated with the two terms in the velocity operator Eq. (8). The canonical part of the velocity operator,  $\mathbf{v}_0 = \mathbf{k}/m$ , yields the charge current  $\mathbf{j}_0 = e \int_{\mathbf{k}, \varepsilon} \frac{\mathbf{k}}{m} \text{Tr}[\hat{w}_{\mathbf{k}\varepsilon}]$ , whose magnetization (curl) component reproduces the normal-metal orbital IFE in the limit  $\alpha_{so} \rightarrow 0$  and, at finite SOC, acquires an additional SOC-dependent correction that we display as  $M_{\text{orb}}^{\text{bare}} - M_{\text{orb}}^{\text{normal}}$  in Fig. 5. In the presence of SOC, however, the spin-dependent component of the velocity operator and the SOC-convective gradient term in the kinetic Eq. 4 introduce two additional current channels that couple the nonequilibrium spin density to charge motion. Accordingly, the orbital magnetization in the Rashba system can be decomposed as

$$M_{\text{orb}}^{\text{total}} = M_{\text{orb}}^{\text{bare}} + M_{\text{orb}}^{\text{SOC-conv}} + M_{\text{orb}}^{\text{SOC-vel}}. \quad (28)$$

Here,  $M_{\text{orb}}^{\text{bare}}$  denotes the orbital response generated by the canonical current  $\mathbf{j}_0$ . This term reduces to the normal-metal orbital IFE in the limit  $\alpha_{so} \rightarrow 0$  and therefore represents the direct generalization of the spinless mechanism discussed in Sec. III A. The quantity plotted in Fig. 4 corresponds to the total orbital response relative to this normal-metal background.

The remaining two terms originate from the spin-orbit component of the velocity operator and represent distinct ways in which SOC modifies the circulating charge currents responsible for the orbital magnetization. Their individual behavior is discussed below.

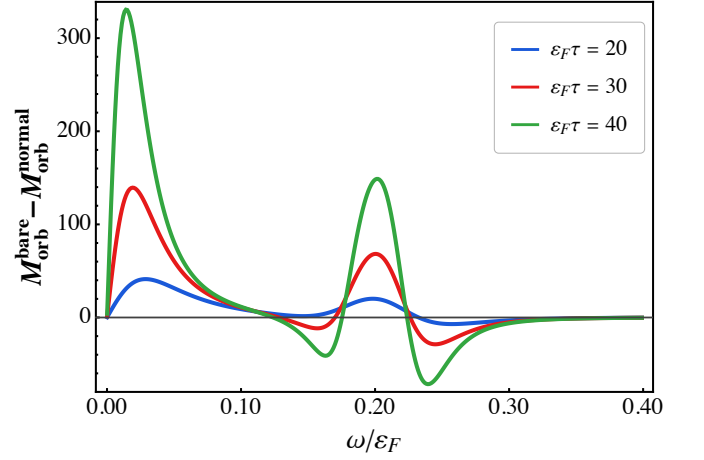


FIG. 5. Plot of dimensionless bare orbital IFE magnetization  $M_{\text{orb}}^{\text{bare}} - M_{\text{orb}}^{\text{normal}}$  vs light frequency normalized by the Fermi energy,  $\omega/\varepsilon_F$  for different values of  $\varepsilon_F\tau$  in 2DEG with Rashba SOC for  $\alpha_{so}k_F/\varepsilon_F = 0.1$ .

### 3. Spin-orbit convective contribution

The first SOC contribution to the orbital inverse Faraday response originates from the gradient term in the kinetic equation,

$$\hat{\mathcal{K}}_{\mathbf{k}\varepsilon}^{(2)} = -\frac{\alpha_{so}}{2} \{(\mathbf{c} \times \hat{\boldsymbol{\sigma}}), \nabla \hat{w}_{\mathbf{k}\varepsilon}\}, \quad (29)$$

which describes the spin-orbit-induced convection of the nonequilibrium distribution function. Although this term does not directly enter the velocity operator, it modifies the spatial structure of the distribution function and thereby affects the canonical charge current  $\mathbf{j}_0 = e \int_{\mathbf{k}, \varepsilon} \frac{\mathbf{k}}{m} \text{Tr}[\hat{w}_{\mathbf{k}\varepsilon}]$ . Physically,  $\hat{\mathcal{K}}^{(2)}$  does not repre-

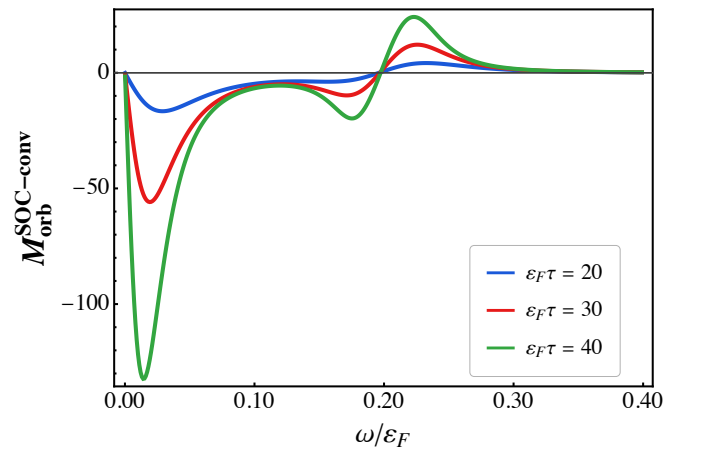


FIG. 6. Plot of dimensionless SOC-induced orbital IFE magnetization  $M_{\text{orb}}^{\text{SOC-conv}}$  vs light frequency normalized by the Fermi energy,  $\omega/\varepsilon_F$  for different values of  $\varepsilon_F\tau$  in 2DEG with Rashba SOC for  $\alpha_{so}k_F/\varepsilon_F = 0.1$ .

sent a new current vertex. Instead it generates a SOC-induced convective distortion of the nonequilibrium distribution function that feeds back into the canonical current  $\mathbf{j}_0$ . Rashba SOC therefore imprints a spin-dependent spatial anisotropy into  $\hat{w}_{\mathbf{k}\varepsilon}(\mathbf{r}, t)$ , which in turn produces an additional transverse (curl) component of the charge current when inserted into  $\mathbf{j}_0 \propto \int (\mathbf{k}/m) \text{Tr}[\hat{w}]$ . We denote the resulting magnetization contribution by  $M_{\text{orb}}^{\text{SOC-conv}}$ .

The frequency dependence of this term is shown in Fig. 6. It shows a sign-reversal at the resonant frequency compared to the bare orbital contribution and its magnitude increases with increasing  $\varepsilon_F \tau$ , reflecting the kinetic origin of the effect: stronger ballistic propagation amplifies the SOC-driven convective distortion of the electronic distribution. In contrast to the bare orbital channel, this contribution therefore arises not from the velocity operator itself but from the SOC-modified convective dynamics of the distribution function entering the canonical current.

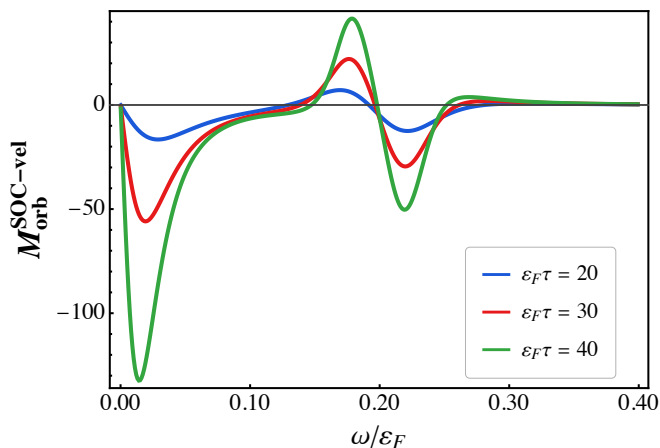


FIG. 7. Plot of SOC-induced orbital IFE magnetization  $M_{\text{orb}}^{\text{SOC-vel}}$  vs light frequency normalized by the Fermi energy,  $\omega/\varepsilon_F$  for different values of  $\varepsilon_F \tau$  in 2DEG with Rashba SOC for  $\alpha_{so} k_F / \varepsilon_F = 0.1$ .

#### 4. SOC-velocity contribution to the orbital IFE

A second SOC contribution to the orbital inverse Faraday response arises directly from the spin-dependent part of the velocity operator

$$\mathbf{v}_{\text{soc}} = \alpha_{\text{so}} (\mathbf{c} \times \boldsymbol{\sigma}), \quad (30)$$

appearing in Eq. (8). Substituting this term into the expression for the electric current density in Eq. 7 produces an additional charge-current channel absent in a normal metal:

$$\mathbf{j}_{\text{soc}} = e \int_{\mathbf{k}, \varepsilon} \text{Tr}[\mathbf{v}_{\text{soc}} \hat{w}_{\mathbf{k}\varepsilon}] = 2e\alpha_{\text{so}} \mathbf{c} \times \mathbf{S}(\mathbf{r}, t). \quad (31)$$

This relation shows that the SOC velocity converts nonequilibrium spin polarization into charge motion, representing the optical analogue of the spin-galvanic effect. For a spatially uniform spin density  $\mathbf{S}$ , this current contributes only to transport. However, once the kinetic dynamics generates finite- $\mathbf{q}$  spin textures in the distribution function, the transverse (curl) component of  $\mathbf{j}_{\text{soc}}$  produces circulating charge flow. The circulating curl component of this current corresponds to an orbital magnetization, which we denote by  $M_{\text{orb}}^{\text{SOC-vel}}$ .

Physically, this mechanism differs from the canonical orbital channel: the circulating currents do not originate from the orbital motion encoded in the velocity  $\mathbf{k}/m$ , but from the direct spin-orbit coupling between spin polarization and charge motion contained in  $\mathbf{v}_{\text{soc}}$ . The resulting frequency dependence of  $M_{\text{orb}}^{\text{SOC-vel}}$  is shown in Fig. 7. Its magnitude grows with increasing  $\varepsilon_F \tau$ , reflecting its kinetic origin in the spin-orbit-coupled dynamics of the nonequilibrium distribution, and over the relevant frequency range it partially compensates the bare orbital contribution generated by the canonical current similar to the convective term.

Combining these contributions yields the total orbital magnetization  $M_{\text{orb}}^{\text{total}}$  shown in Fig. 4. Although an orbital inverse Faraday effect already exists in a normal metal, Rashba spin-orbit coupling strongly modifies its magnitude and frequency dependence. In particular, when the radiation frequency approaches the Rashba spin splitting at the Fermi surface,  $\omega \sim 2\alpha_{so} k_F$ , both spin and orbital responses exhibit a pronounced resonance enhancement. While the canonical orbital contribution provides the baseline response, the SOC-generated channels grow with increasing quasiparticle lifetime and become significant near the spin-orbit resonance. The inverse Faraday response of a Rashba metal therefore reflects the combined action of spin polarization and circulating charge currents, with spin-orbit coupling introducing additional channels that enhance the light-induced magnetization.

## IV. DISCUSSION

The results presented above clarify that the inverse Faraday response of a Rashba metal cannot be understood solely as a spin response. Although earlier treatments of the Rashba IFE emphasized the spin channel generated by spin-orbit coupling [59–63], our analysis shows that the orbital channel is an essential and independently identifiable part of the response. In particular, the orbital contribution reduces smoothly to the normal-metal result as  $\alpha_{so} \rightarrow 0$ , so any consistent theory of the inverse Faraday effect in spin-orbit-coupled metals must recover this normal-state orbital contribution in the weak-SOC limit.

A central advantage of the present formulation is that it separates spin polarization from circulating charge currents at the level of physical observables. Spin magne-

tization is obtained directly from the spin trace of the nonequilibrium Wigner distribution function, whereas orbital magnetization is extracted from the curl component of the nonlinear charge current. This separation is important because the presence of a light-induced current vertex does not by itself imply orbital magnetization: only the circulating part of the current contributes to the orbital moment. By working directly with the current decomposition implied by the full velocity operator, we are able to identify which parts of the response correspond to genuine magnetization currents and which correspond only to transport. This makes the distinction between spin and orbital contributions transparent in the calculated response.

Within this framework, Rashba spin-orbit coupling modifies the orbital inverse Faraday effect in two distinct ways. First, the spin-dependent part of the velocity operator generates an additional current channel,  $\mathbf{j}_{\text{soc}}$ , which converts nonequilibrium spin polarization into charge motion. Second, the SOC gradient term in the kinetic equation produces a convective distortion of the nonequilibrium distribution function, which feeds back into the canonical current and generates an additional circulating contribution. These two SOC-enabled channels do not replace the normal-metal orbital response; rather, they add to it and reshape its frequency dependence. The total orbital magnetization in the Rashba system should therefore be viewed as the sum of a normal-metal baseline and SOC-induced corrections.

Another important conclusion is the role of disorder. In the present theory, disorder does not generate the inverse Faraday response; instead, it controls its magnitude through the momentum relaxation time. Both the spin and orbital contributions are suppressed by stronger disorder and enhanced in cleaner systems. The peak structure that appears in the normal-metal orbital response at  $\omega \sim \tau^{-1}$  reflects the competition between finite-frequency driving and momentum relaxation, while in

the Rashba case an additional resonance appears when the radiation frequency approaches the spin splitting at the Fermi surface,  $\omega \simeq 2\alpha_{\text{so}}k_F$ . Near this resonance, both spin and orbital channels are enhanced, and the SOC-induced orbital terms become particularly important.

More broadly, the present results highlight that the inverse Faraday effect in conducting systems should be viewed as a nonlinear response involving both spin polarization and circulating charge currents. Because Rashba two-dimensional electron gases are realized in semiconductor heterostructures and oxide interfaces, the predicted resonance structure and the sensitivity of the response to quasiparticle lifetime may be relevant for future ultrafast magneto-optical and helicity-dependent transport measurements. Even if separating spin and orbital contributions experimentally remains challenging, their different dependence on disorder, frequency, and spin-orbit coupling may provide indirect signatures of their interplay. In this sense, the present analysis may serve as a useful theoretical reference point for a variety of nonlinear light-matter phenomena currently explored experimentally, including light-induced magnetism, superconductivity, dynamical multiferroicity, and related opto-spintronic and orbitronic device concepts [75–80].

## ACKNOWLEDGMENTS

We thank Jigang Wang and Maxim Dzero for discussions. J.H. and C.S. are supported by Ames National Laboratory and Iowa State University start-up funds.

## Appendix A: Analytic Expressions

Analytic expression of  $\mathbf{M}_{\text{spin}}$  is given by

$$\mathbf{M}_{\text{spin}} = i(\mathbf{E}_0 \times \mathbf{E}_0^*) \text{Im} \left[ \frac{e^3 \tau}{32m^2 \pi \alpha_{\text{so}}^2 \omega^2 z_{\omega,-} (1 - z_{\omega,-} \tau)} \left( \frac{1}{\tau^3} \log f_1 \left( \frac{1}{\tau} \right) - z_{\omega,-}^3 \log f_1(z_{\omega,-}) \right) + \frac{e^3}{8m\pi\tau\omega^2 z_{\omega,-}} \tan^{-1} \frac{512m^3 \alpha_{\text{so}}^6 (1 + 4\zeta^2) \tau^5 \omega^2}{\left( (1 + 4\zeta^2)^2 + 16m^2 \alpha_{\text{so}}^4 \tau^2 \right)^2 - 64(m\omega \alpha_{\text{so}}^2 \tau^2)^2 \left( (1 + 4\zeta^2)^2 - 16m^2 \alpha_{\text{so}}^4 \tau^2 \right)} \right], \quad (\text{A1})$$

where  $\zeta = \alpha_{\text{so}} k_F \tau$ ,  $z_{\omega,\pm} = \mp i\omega + 1/\tau$  and  $f_1(z)$  is given by

$$f_1(z) = \frac{\left( (z^2 + 4k_F^2 \alpha_{\text{so}}^2)^2 + 16m^2 z^2 \alpha_{\text{so}}^4 \right)^2}{\left( (z^2 + 4k_F^2 \alpha_{\text{so}}^2)^2 + 16m^2 z^2 \alpha_{\text{so}}^4 - 64m^2 \alpha_{\text{so}}^4 \omega^2 \right)^2 + 4096m^4 \alpha_{\text{so}}^8 z^2 \omega^2} \quad (\text{A2})$$

Analytic expression of  $M_{\text{orb}}^{\text{bare}}$  is given by

$$M_{\text{orb}}^{\text{bare}} = i (\mathbf{E}_0 \times \mathbf{E}_0^*) \text{Im} \frac{e^3 \tau}{512 \pi m^2 z_{\omega,+}^2} \left[ 256 k_F^2 + 640 m^2 \alpha_{so}^2 + \frac{m^2}{\omega^2} [2f_2(0) - f_2(\omega) - f_2(-\omega)] \right. \\ \left. + \frac{3z_{\omega,+}^4}{\alpha_{so}^2 \omega^2} \log \frac{2g(0)}{g(\omega)g(-\omega)} \right], \quad (\text{A3})$$

where  $f_2[\pm\omega]$  and  $g[\pm\omega]$  is given by

$$f_2[\pm\omega] = \frac{4z_{\omega,+}^6 (z_{\omega,+}^2 + 4\alpha_{so}^2 (k_F^2 + 2m(m\alpha_{so}^2 \pm \omega)))}{m^2 \alpha_{so}^2 \left( (z_{\omega,+}^2 + 4(k_F^2 \pm 2m\omega)\alpha_{so}^2)^2 + 16m^2 z_{\omega,+}^2 \alpha_{so}^4 \right)}, \quad (\text{A4}) \\ g[\pm\omega] = (z_{\omega,+}^2 + 4(k_F^2 \pm 2m\omega)\alpha_{so}^2)^2 + 16m^2 z_{\omega,+}^2 \alpha_{so}^4.$$

- 
- [1] L. P. Pitaevskii, Electric Forces in a Transparent Dispersive Medium, *JETP* **12**, 1008 (1960).
- [2] P. S. Pershan, Nonlinear optical properties of solids: Energy considerations, *Phys. Rev.* **130**, 919 (1963).
- [3] J. P. van der Ziel, P. S. Pershan, and I. D. Malmstrom, Optically-Induced Magnetization Resulting from the Inverse Faraday Effect, *Phys. Rev. Lett.* **15**, 190 (1965).
- [4] P. S. Pershan, J. P. van der Ziel, and L. D. Malmstrom, Theoretical Discussion of the Inverse Faraday Effect, Raman Scattering, and Related Phenomena, *Phys. Rev.* **143**, 574 (1966).
- [5] P. I. Nikitin and A. I. Savchuk, The faraday effect in semimagnetic semiconductors, *Soviet Physics Uspekhi* **33**, 974 (1990).
- [6] C. A. Perroni and A. Liebsch, Coherent control of magnetization via inverse faraday effect, *Journal of Physics: Condensed Matter* **18**, 7063 (2006).
- [7] C. A. Perroni and A. Liebsch, Magnetization dynamics in dysprosium orthoferrites via the inverse faraday effect, *Phys. Rev. B* **74**, 134430 (2006).
- [8] M. I. Kurkin, N. B. Bakulina, and R. V. Pisarev, Transient inverse faraday effect and ultrafast optical switching of magnetization, *Phys. Rev. B* **78**, 134430 (2008).
- [9] D. Popova, A. Bringer, and S. Blügel, Theoretical investigation of the inverse faraday effect via a stimulated raman scattering process, *Phys. Rev. B* **85**, 094419 (2012).
- [10] S. Takayoshi, H. Aoki, and T. Oka, Magnetization and phase transition induced by circularly polarized laser in quantum magnets, *Phys. Rev. B* **90**, 085150 (2014).
- [11] M. Battiato, G. Barbalinardo, and P. M. Oppeneer, Quantum theory of the inverse faraday effect, *Phys. Rev. B* **89**, 014413 (2014).
- [12] A. V. Kimel, A. Kirilyuk, P. A. Usachev, R. V. Pisarev, A. M. Balbashov, and T. Rasing, Ultrafast non-thermal control of magnetization by instantaneous photomagnetic pulses, *Nature* **435**, 655 (2005).
- [13] A. Kirilyuk, A. Kimel, F. Hansteen, T. Rasing, and R. V. Pisarev, Ultrafast all-optical control of the magnetization in magnetic dielectrics, *Low Temperature Physics* **32**, 748 (2006).
- [14] V. V. Kruglyak, Use of the faraday optical transformer for ultrafast magnetization reversal of nanomagnets, *Journal of Nanophotonics* **1**, 013502 (2007).
- [15] T. Satoh, S.-J. Cho, T. Shimura, K. Kuroda, H. Ueda, Y. Ueda, and M. Fiebig, Photoinduced transient faraday rotation in nio, *Journal of the Optical Society of America B* **27**, 1421 (2010).
- [16] A. H. M. Reid, A. V. Kimel, A. Kirilyuk, J. F. Gregg, and T. Rasing, Investigation of the femtosecond inverse faraday effect using paramagnetic  $\text{dy}_3\text{al}_5\text{o}_{12}$ , *Phys. Rev. B* **81**, 104404 (2010).
- [17] A. Kirilyuk, A. V. Kimel, and T. Rasing, Ultrafast Optical Manipulation of Magnetic Order, *Rev. Mod. Phys.* **82**, 2731 (2010).
- [18] R. V. Mikhaylovskiy, E. Hendry, and V. V. Kruglyak, Ultrafast inverse faraday effect in a paramagnetic terbium gallium garnet crystal, *Phys. Rev. B* **86**, 100405 (2012).
- [19] J. Wätzel, P. c. v. Rebernik Ribič, M. Coreno, M. B. Danailov, C. David, A. Demidovich, M. Di Fraia, L. Giannessi, K. Hansen, i. c. v. Krušič, M. Manfredda, M. Meyer, A. Mihelič, N. Mirian, O. Plekan, B. Ressel, B. Rösner, A. Simoncig, S. Spampinati, M. Stupar, M. c. v. Žitnik, M. Zangrando, C. Callegari, J. Berakdar, and G. De Ninno, Light-induced magnetization at the nanoscale, *Phys. Rev. Lett.* **128**, 157205 (2022).
- [20] Z. Jin, H. Ma, D. Li, G. Ma, M. Wang, and C. Zhao, Femtosecond inverse faraday effect in magnetic ionic liquid [bmim]fecl<sub>4</sub>, *Journal of Applied Physics* **109**, 073109 (2011).
- [21] V. V. Pavlov, R. V. Pisarev, S. G. Nefedov, I. A. Akimov, D. R. Yakovlev, M. Bayer, A. B. Henriques, P. H. O. Rappl, and E. Abramof, Magnetic-field-induced crossover from the inverse faraday effect to the optical orientation in eute, *Journal of Applied Physics* **123**, 193102 (2018).
- [22] F. Guo, Y. Sun, X. Yang, X. Chen, B. Zhao, N. Zhuang, and J. Chen, Growth, faraday and inverse faraday characteristics of  $\text{tb}_2\text{ti}_2\text{o}_7$  crystal, *Optics Express* **24**, 5734 (2016).
- [23] V. H. Ortiz, S. B. Mishra, L. Vuong, S. Coh, and R. B. Wilson, Specular inverse faraday effect in transition metals, *Phys. Rev. Mater.* **7**, 125202 (2023).
- [24] D. Hinzke, M. Berritta, U. Atxitia, R. Mondal, P. M. Oppeneer, and U. Nowak, Inverse faraday effect as mechanism for ultrafast all-optical magnetic switching, in *2015 IEEE International Magnetics Conference (INTERMAG)* (2015) pp.

- 1–1.
- [25] T. Danegger, M. Berritta, K. Carva, S. Selzer, U. Ritzmann, P. M. Oppeneer, and U. Nowak, Ultrafast coherent all-optical switching of an antiferromagnet with the inverse faraday effect, *Phys. Rev. B* **104**, L060413 (2021).
- [26] M. Köhlmann, L. Vollroth, K. Jäckel, K. Hovorakova, E. Schmoranzero, K. Carva, D. Hinzke, U. Nowak, M. Münzenberg, and J. Walowski, Exploring the impact of the inverse faraday-effect on all-optical helicity-dependent magnetization switching, *Journal of Applied Physics* **138**, 043901 (2025).
- [27] O. Huber, K. Kuhlbrodt, E. Anderson, W. Li, K. Watanabe, T. Taniguchi, M. Kroner, X. Xu, A. Imamoğlu, and T. Smoleński, Optical control over topological chern number in moiré materials, *Nature* **649**, 1153 (2026).
- [28] R. Hertel, Theory of the inverse faraday effect in metals, *Journal of Magnetism and Magnetic Materials* **303**, L1 (2006).
- [29] H.-L. Zhang, Y.-Z. Wang, and X.-J. Chen, A simple explanation for the inverse faraday effect in metals, *Journal of Magnetism and Magnetic Materials* **321**, L73 (2009).
- [30] R. Hertel and M. Fähnle, Macroscopic drift current in the inverse faraday effect, *Phys. Rev. B* **91**, 020411 (2015).
- [31] T. Yoshino, Simple theory of the inverse faraday effect with relationship to optical constants  $n$  and  $k$ , *Journal of Magnetism and Magnetic Materials* **323**, 2531 (2011).
- [32] I. Petrila, F. Ungureanu, and V. Manta, Effects of laser beam modulation on all-optical switching phase diagrams in magneto-optical ultrafast storage device, *Journal of Computational Electronics* **14**, 627 (2015).
- [33] M. Merte, F. Freimuth, D. Go, T. Adamantopoulos, F. R. Lux, L. Plucinski, O. Gomonay, S. Blügel, and Y. Mokrousov, Photocurrents, inverse faraday effect, and photospin hall effect in  $\text{mn}_2\text{au}$ , *APL Materials* **11**, 071106 (2023).
- [34] T. Yokoyama, Creation of Superconducting Vortices by Angular Momentum of Light, *J. Phys. Soc. Jpn.* **89**, 103703 (2020).
- [35] S. V. Mironov, A. S. Mel'nikov, I. D. Tokman, V. Vadimov, B. Lounis, and A. I. Buzdin, Inverse faraday effect for superconducting condensates, *Phys. Rev. Lett.* **126**, 137002 (2021).
- [36] A. H. Majedi, Microwave-Induced Inverse Faraday Effect in Superconductors, *Phys. Rev. Lett.* **127**, 087001 (2021).
- [37] M. D. Croitoru, B. Lounis, and A. I. Buzdin, Influence of a nonuniform thermal quench and circular polarized radiation on spontaneous current generation in superconducting rings, *Phys. Rev. B* **105**, L020504 (2022).
- [38] V. D. Plastovets, I. D. Tokman, B. Lounis, A. S. Mel'nikov, and A. I. Buzdin, All-optical generation of Abrikosov vortices by the inverse Faraday effect, *Phys. Rev. B* **106**, 174504 (2022).
- [39] I. D. Tokman, Q. Chen, I. A. Shereshevsky, V. I. Pozdnyakova, I. Oladyshkin, M. Tokman, and A. Belyanin, Inverse faraday effect in graphene and weyl semimetals, *Phys. Rev. B* **101**, 174429 (2020).
- [40] S. Banerjee, U. Kumar, and S.-Z. Lin, Inverse faraday effect in mott insulators, *Phys. Rev. B* **105**, L180414 (2022).
- [41] V. I. Belotelov, E. A. Bezus, L. L. Doskolovich, A. N. Kalish, and A. K. Zvezdin, Inverse faraday effect in plasmonic heterostructures, *Journal of Physics: Conference Series* **200**, 092003 (2010).
- [42] A. Nadarajah and M. T. Sheldon, Optoelectronic phenomena in gold metal nanostructures due to the inverse faraday effect, *Optics Express* **25**, 12753 (2017).
- [43] J. Hurst, P. M. Oppeneer, G. Manfredi, and P.-A. Hervieux, Magnetic moment generation in small gold nanoparticles via the plasmonic inverse Faraday effect, *Phys. Rev. B* **98**, 134439 (2018).
- [44] A. K. González-Alcalde, X. Shi, V. H. Ortiz, J. Feng, R. B. Wilson, and L. T. Vuong, Enhanced inverse faraday effect and time-dependent thermo-transmission in gold nanodisks, *Nanophotonics* **13**, 1993 (2024).
- [45] S. Parchenko, K. Hoffhuis, A. Å. Larsson, V. Kapaklis, V. Scagnoli, L. J. Heyderman, and A. Kleibert, Plasmon-enhanced optical control of magnetism at the nanoscale via the inverse faraday effect, *Advanced Photonics Research* **6**, 2400083 (2025).
- [46] C. Hareau, X. Yang, M. Sanz-Paz, M. Sheldon, and M. Mivelle, Engineering magnetization with photons: Nanoscale advances in the inverse faraday effect for metallic and plasmonic architectures, *ACS Photonics* **12**, 6535 (2025).
- [47] S. Hamidi, M. Razavinia, and M. Tehranchi, Enhanced optically induced magnetization due to inverse faraday effect in plasmonic nanostructures, *Optics Communications* **338**, 240 (2015).
- [48] S.-J. Im, C.-S. Ri, K.-S. Ho, and J. Herrmann, Third-order nonlinearity by the inverse faraday effect in planar magnetoplasmonic structures, *Phys. Rev. B* **96**, 165437 (2017).
- [49] C.-S. Ri, S.-J. Im, J.-S. Pae, K.-S. Ho, Y.-H. Han, and J. Herrmann, Nanoscale magnetization and third-order nonlinearity by the plasmon-induced inverse faraday effect in graphene-covered semiconductors, *Phys. Rev. B* **100**, 155404 (2019).
- [50] D. M. Krichevsky, V. A. Ozerov, A. V. Bel'kova, D. A. Sylgacheva, A. N. Kalish, S. A. Evstigneeva, A. S. Pakhomov, T. V. Mikhailova, S. D. Lyashko, A. L. Kudryashov, E. Y. Semuk, A. I. Chernov, V. N. Berzhansky, and V. I. Belotelov, Spatially inhomogeneous inverse faraday effect provides tunable nonthermal excitation of exchange dominated spin waves, *Nanophotonics* **13**, 299 (2024).
- [51] D. M. Krichevsky, D. O. Ignatyeva, and V. I. Belotelov, Inverse faraday effect at mie resonances, *Phys. Rev. Appl.* **22**, 064087 (2024).
- [52] Y. Mou, X. Yang, B. Gallas, and M. Mivelle, A chiral inverse faraday effect mediated by an inversely designed plasmonic antenna, *Nanophotonics* **12**, 2115 (2023).
- [53] X. Yang, Y. Mou, R. Zapata, B. Reynier, B. Gallas, and M. Mivelle, An inverse faraday effect generated by linearly polarized light through a plasmonic nano-antenna, *Nanophotonics* **12**, 687 (2023).
- [54] X. Yang, *Manipulating the inverse Faraday effect at the nanoscale*, Theses, Sorbonne Université (2024).
- [55] V. M. Edelstein, Inverse faraday effect in conducting crystals caused by a broken mirror symmetry, *Phys. Rev. Lett.* **80**, 5766 (1998).
- [56] V. Edelstein, Spin polarization of conduction electrons induced by electric current in two-dimensional asymmetric electron systems, *Solid State Communications* **73**, 233 (1990).
- [57] V. M. Edelstein, Magnetoelectric effect in polar superconductors, *Phys. Rev. Lett.* **75**, 2004 (1995).
- [58] V. M. Edelstein, Magnetoelectric effect in dirty superconductors with broken mirror symmetry, *Phys. Rev. B* **72**, 172501 (2005).
- [59] K. Taguchi and G. Tatara, Theory of inverse faraday effect in a disordered metal in the terahertz regime, *Phys. Rev.*

- B **84**, 174433 (2011).
- [60] K. Taguchi and G. Tatara, Theory of inverse faraday effect in rashba system, *Journal of Physics: Conference Series* **400**, 042055 (2012).
- [61] A. Qaiumzadeh and M. Titov, Theory of light-induced effective magnetic field in rashba ferromagnets, *Phys. Rev. B* **94**, 014425 (2016).
- [62] Y. Tanaka, T. Inoue, and M. Mochizuki, Theory of the inverse faraday effect due to the rashba spin-orbit interactions: roles of band dispersions and fermi surfaces, *New Journal of Physics* **22**, 083054 (2020).
- [63] M. Tanaka and M. Sato, Theory of the inverse faraday effect in dissipative rashba electron systems: Floquet engineering perspective, *Phys. Rev. B* **110**, 045204 (2024).
- [64] S. B. Mishra and S. Coh, Spin contribution to the inverse faraday effect of nonmagnetic metals, *Phys. Rev. B* **107**, 214432 (2023).
- [65] S. B. Mishra, Inverse faraday effect in  $3d$ ,  $4d$ , and  $5d$  transition metals, *Phys. Rev. B* **111**, 174413 (2025).
- [66] P. Sharma and A. V. Balatsky, Light-induced orbital magnetism in metals via inverse faraday effect, *Phys. Rev. B* **110**, 094302 (2024).
- [67] M. Dzero, Inverse faraday effect in superconductors with potential impurities, *Phys. Rev. B* **110**, 054506 (2024).
- [68] M. Dzero, Inverse faraday effect in disordered two-dimensional electronic systems, *Phys. Rev. Lett.* **135**, 116902 (2025).
- [69] P. J. Wong, I. M. Khaymovich, G. Aeppli, and A. V. Balatsky, Large inverse faraday effect for rydberg states of free atoms and isolated donors in semiconductors, *Phys. Rev. B* **111**, 064425 (2025).
- [70] M. D. Croitoru, S. V. Mironov, B. Lounis, and A. I. Buzdin, Toward the Light-Operated Superconducting Devices: Circularly Polarized Radiation Manipulates the Current-Carrying States in Superconducting Rings, *Advanced Quantum Technologies* **82**, 2200054 (2022).
- [71] X.-J. Chen, Fundamental mechanism for all-optical helicity-dependent switching of magnetization, *Sc. Reps.* **7**, 41294 (2017).
- [72] E. G. Mishchenko, A. V. Shytov, and B. I. Halperin, Spin current and polarization in impure two-dimensional electron systems with spin-orbit coupling, *Phys. Rev. Lett.* **93**, 226602 (2004).
- [73] A. V. Shytov, E. G. Mishchenko, H.-A. Engel, and B. I. Halperin, Small-angle impurity scattering and the spin hall conductivity in two-dimensional semiconductor systems, *Phys. Rev. B* **73**, 075316 (2006).
- [74] M. Dzero, J. Hasan, and A. Levchenko, Resonant second harmonic generation in a two-dimensional electron system, *Phys. Rev. B* **112**, 045416 (2025).
- [75] X. Wang, C. Xiao, H. Park, J. Zhu, C. Wang, M. T. Taniguchi, K. Watanabe, J. Yan, D. Xiao, D. R. Gamelin, W. Yao, and X. Xu, Light-induced Ferromagnetism in Moiré Superlattices, *Nature* **604**, 468 (2022).
- [76] D. Fausti, R. Tobey, N. Dean, S. Kaiser, A. Dienst, M. C. Hoffmann, S. Pyon, T. Takayama, H. Takagi, and A. Cavalleri, Light-induced superconductivity in a stripe-ordered cuprate, *Science* **331**, 189 (2011).
- [77] D. M. Juraschek, M. Fechner, A. V. Balatsky, and N. A. Spaldin, Dynamical multiferroicity, *Phys. Rev. Mater.* **1**, 014401 (2017).
- [78] A. Kogar *et al.*, Light-induced charge density wave in *LaTe<sub>3</sub>*, *Nat. Phys.* **16**, 159 (2020).
- [79] G. Shaw, S. Blanco Alvarez, J. Brisbois, L. Burger, L. B. Pinheiro, R. B. Kramer, M. Motta, K. Fleury-Frenette, W. Ortiz, B. Vanderheyden, and A. Silhanek, Magnetic Recording of Superconducting States, *Metals* **9**, 1022 (2019).
- [80] A. Kimel *et al.*, 2022 Magneto-Optics RoadMap, *J. Phys. D: Appl. Phys.* **55**, 463003 (2022).
- [81] T. Kita, Gauge invariance and Hall terms in the quasi-classical equations of superconductivity, *Phys. Rev. B* **64**, 054503 (2001).